A General Pattern of Assisted Flux Barriers for Design Optimization of an Asymmetric V-shape Interior Permanent Magnet Machine

Yanding Bi[1], Jiahui Huang[1], Huihuan Wu[1], Weinong Fu[2], Shuangxia Niu[1], *Senior Member, IEEE,* and Xing Zhao[3], *Member, IEEE*

[1]Department of Electrical Engineering, The Hong Kong Polytechnic University, Hong Kong, eesxniu@polyu.edu.hk
[2]Shenzhen Institutes of Advanced Technology, Chinese Academy of Sciences, Shenzhen 518055, China, wn.fu@siat.ac.cn
[3]Department of Electronic Engineering, University of York, United Kingdom, xing.zhao@york.ac.uk

In this work, a novel general pattern of assisted flux barriers in an asymmetric V-shape interior permanent magnet (AVIPM) machine is presented. The AVIPM machine has a symmetric permanent magnet (PM) structure and an asymmetric rotor core structure to realize the magnetic-field-shifting (MFS) effect. The general pattern can represent four possible types of assisted flux barriers at different positions on the rotor core and the final structure can be automatically determined by using optimization method. The advantage of the proposed optimization pattern is that the optimal design of assisted flux barriers in V-shape interior permanent magnet (VIPM) machines with high torque and low torque ripple can be generated within a short computing time. The proposed optimization method is applied to improve the structure of a conventional 8-pole 48-slot VIPM machine, which is commonly used for driving electric vehicles (EVs). A non-dominated sorting genetic algorithm II (NSGA-II) is used for the global optimization of both a VIPM machine and an AVIPM machine. The electromagnetic performance is computed using a finite element analysis (FEA). Moreover, a frozen permeability (FP) method is applied to perform an accurate separation of PM torque and reluctance torque. The results exhibit that the peak output torque of the AVIPM machine is increased by 8.7% compared to a conventional VIPM machine with the same PM volume due to the notable MFS effect. In the meantime, the AVIPM machine has a better overload capability due to the larger contribution of reluctance torque. Moreover, the proposed machine has high efficiency of over 97%.

***Index Terms*—Finite element analysis (FEA), optimization, permanent magnet machines, permeability, torque.**

I. Introduction

PERMANENT magnet synchronous machines (PMSMs) have intrinsic advantages of high torque density and high efficiency due to the usage of permanent magnets (PMs) as the field source of magnetic excitation. In a PMSM, the PM is either mounted on the surface of the rotor or inserted into the rotor cavity. Thus, PMSMs can be classified as surface-mounted PM (SPM) machines and interior PM (IPM) machines. The IPM machines can offer high power density, high efficiency, extended constant power-speed range (CPSR), and superior rotor mechanical robustness [1].

Recently, a novel approach was proposed in the literature to enhance torque density of PMSMs, which is designated as magnetic-field-shifting (MFS) effect [2-4]. MFS effect is a design concept to increase the resultant torque by decreasing the current phase angle difference between the maximum values of magnetic torque and reluctance torque. MFS effect can be realized by asymmetric configurations of IPM machines. However, the structures of asymmetric IPM (AIPM) machines are very difficult to be determined by designer's experience.

The research in this work focuses on AIPM machines with a symmetric V-shape PM configuration and an asymmetric rotor core configuration. The rotor asymmetry is constructed by employing assisted flux barriers on one side of the V-shape cavity. To the best of the authors' knowledge, all reported asymmetric V-shape IPM (AVIPM) machines employ only one type of assisted flux barrier on rotor topology [3-6]. With the purpose to investigate the optimized structure of rotor core topology, a novel general pattern of assisted flux barriers on rotor core of V-shape IPM (VIPM) machines is proposed in this paper, which includes the existing flux barriers in the literature. Four types of assisted flux barriers located at different positions can be represented and the final structure can be determined automatically using optimization. The general pattern is employed in a conventional VIPM machine. The conventional VIPM machine and the proposed AVIPM machine are shown in Fig. 1. The novel AVIPM machine with multiple asymmetric flux barriers has an 8.7% higher maximum torque than the conventional VIPM machine with a same PM volume. The performance analysis reveals the effectiveness of MFS in improving output torque.

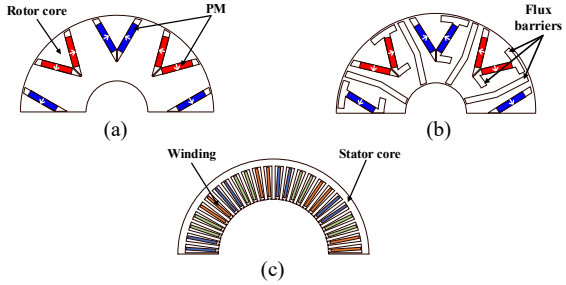

Fig. 1. (a) Rotor structure of conventional V-shape IPM machine. (b) Rotor structure of asymmetric V-shape IPM machine. (c) Stator structure of the 8-pole 48-slot PM synchronous machine.

II. Proposed Configuration and Optimal Design

A. General Pattern of Assisted Flux Barriers in AVIPM Machine

Fig. 2 presents the proposed general pattern of assisted flux barriers in the AVIPM machine. As shown in Fig. 2 (a), four different types of assisted flux barriers can be generated using

This article has been accepted for publication in a future issue of this journal, but has not been fully edited. Content may change prior to final publication. Citation information: DOI 10.1109/TMAG.2022.3159960, IEEE Transactions on Magnetics

this general pattern. Fig. 2 (b) shows the rotor core structures with one of the four types of flux barriers. The flux barriers can locate at the outer end of the V-shape cavity (FB_1 and FB_2) [3-5], the inner end of the V-shape cavity (FB_3), or the area between two V-shape cavities in one pole-pair (FB_4) [6]. In the meantime,the effect of placing multiple flux barriers on the rotor core can also be investigated with the proposed general pattern. The possible topologies of the AVIPM rotor are shown in Fig.1 (b).

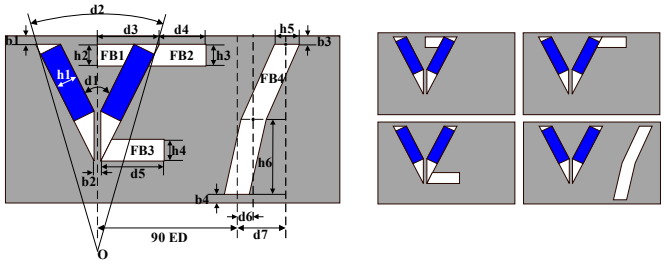

(a) (b)

Fig. 2. (a) The general pattern of asymmetric flux barriers. (b) The flux barriers generated by the general pattern.

The general design parameters of the conventional VIPM machine and the proposed AVIPM machine are shown in Table I. The machines have the same stator outer diameter of 220 mm, stack length of 50 mm, and airgap length of 0.8 mm.The pole-pair numbers and stator slot numbers are 4 and 48, respectively. A single-layer distributed winding is adopted for both machines.

TABLE I
GENERAL DESIGN PARAMETERS OF THE MACHINES

Parameters	Values
Axial length, L_a (mm)	50
Outer diameter of stator, D_{sout} (mm)	220
Length of airgap, T_a (mm)	0.8
Number of pole-pairs, P_s(mm)	4
Number of slots, N_s(mm)	48
Inner diameter of stator, D_{sin}(mm)	126.8
Current density, (A/mm^2)	6.0
Slot filling factor	0.5
Number of conductors	10
PM volume, (mm^3)	64400
PM material	Nd38EH
Steel material	DW310-35

B. Principle of Magnetic-field-shifting Effect

In conventional IPM machines, the resultant torque is composed of two components, namely the PM torque and reluctance torque. The resultant torque can be expressed as:

$$T_e = T_{pm} + T_r = \frac{3p}{2}\left[\psi_{pm} i_s \cos\beta + \frac{1}{2}(L_q - L_d) i_s^{\,2} \sin 2\beta\right] \quad (1)$$

where T_e, T_{pm}, and T_r are the resultant torque, PM torque and reluctance torque, respectively. P is the pole-pair number, ψ_{pm} is the PM flux linkage, i_s is the amplitude of phase current, and β is the current phase angle. L_d and L_q are d- and q-axis inductances, respectively. As shown in (1), the current phase angles of the peak value of PM torque and reluctance torque are separated by 45 electrical degrees (ED). Thus, only a portion of PM torque and reluctance torque is utilized at the peak resultant torque.

The resultant torque of AIPM machines can be expressed as:

$$T_e = \frac{3p}{2}\left[\psi_{pm} i_s \cos(\beta - \alpha_s) + \frac{1}{2}(L_q - L_d) i_s^{\,2} \sin 2\beta\right] \quad (2)$$

The shifting angle of PM flux linkage can be denoted as α_s [7]. The MFS effect reduces the current angle difference between the maximum values of PM torque and reluctance torque, which improves peak torque.

C. Design Optimization of Machines

To perform a fair comparison, the conventional VIPM machine and the proposed AVIPM machine are both optimized with a same PM volume. Firstly, the VIPM machine is globally optimized to decide the design parameters of both stator and rotor. Then, the values of stator parameters are fixed, and the rotor parameters of the AVIPM machine are optimized. The reason for performing optimization in this sequence is to demonstrate the MFS effect resulting from the asymmetric rotor core and eliminate the influence of stator parameters on machine performance.

The non-dominated sorting genetic algorithm II (NSGA-II) method is applied in this study, which imitates the natural selection process [8]. The optimization process is shown in Fig. 3. Two objective functions, including maximizing average torque and minimizing torque ripple, are evaluated using the finite element analysis (FEA). The population with high ranking are reproduced in the next generation. To produce diversified population, crossover and mutation are adopted. The VIPM machine has 10 optimization variables, and the AVIPM machine has 15. The number of populations and generations are 120 and 100, respectively. The crossover factor is 0.9, and the mutation factor is 0.1. The main optimal values of both machines are shown in Table II.

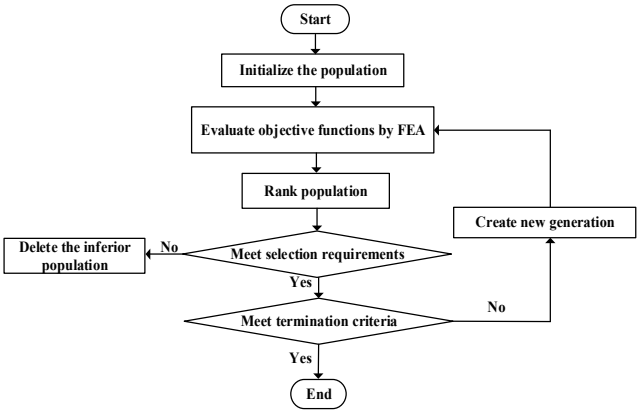

Fig. 3. The flowchart of the global optimization process by using NSGA-II and FEA.

III. COMPARISON OF MACHINE PERFORMANCES

The performances of the optimized VIPM machine and the AVIPM machine are analyzed and compared in this section. The open-circuit characteristics, including the flux distribution, air gap flux density, and the phase back emf, are discussed first. Then, the on-load torque performance is presented and

compared, which reveals the merits of the MFS effect generated by the asymmetric rotor topology.

TABLE II
MAIN OPTIMIZED PARAMETERS OF VIPM MACHINE AND AVIPM MACHINE

Parameters	Optimal values of VIPM	Optimal values of AVIPM
Length of stator yoke, T_{sy}(mm)	8.3	
Length of stator tooth, H_t(mm)	38.3	
Width of stator tooth, W_t(mm)	3.6	
d_1 (degree)	66.1	66.5
d_2 (degree)	30.8	29.9
d_3 (degree)	/	0
d_4 (degree)	/	6.8
d_5 (degree)	/	19.6
d_6 (degree)	/	10.1
d_7 (degree)	/	5.3
h_1 (mm)	4.14	0
h_2 (mm)	/	4
h_3 (mm)	/	4.5
h_4 (mm)	/	5.3
h_5 (mm)	/	1
h_6 (mm)	/	30
b_1 (mm)	0.95	0.95
b_2 (mm)	0.5	0.5
b_3 (mm)	/	1.3
b_4 (mm)	/	1.1

A. The Open-circuit Performance of Machines

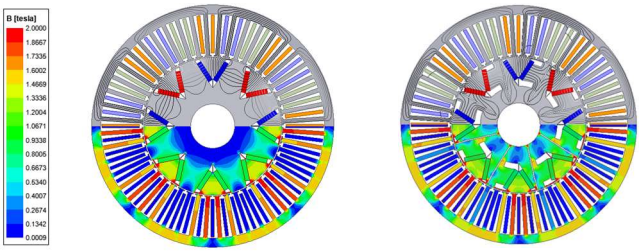

(a) (b)

Fig. 4. FEA results of open-circuit flux distribution and flux density of the optimized machines. (a) VIPM. (b) AVIPM.

The optimized structures of the VIPM machine and the AVIPM machine are shown in Fig. 4. As shown in Table II, the values of d_3 and h_2 are 0, and the value of h_5 is small, which means FB_1 and FB_4 have little influence on the production of the MFS effect. As a result, the FB_2 and FB_3 are the main flux barriers on the optimized rotor core of the AVIPM machine, as shown in Fig. 4 (b).

The open-circuit flux distribution is also shown in Fig. 4. Compared with the symmetric flux distribution of the VIPM machine, the AVIPM machine has an asymmetric PM flux distribution due to the existence of flux barriers. The airgap flux density waveform and the harmonic distribution are shown in Fig. 5. Due to the flux barriers, the AVIPM machine has a larger main flux compared with that of the VIPM machine, as shown in Fig. 5 (b). The phase back electromotive force (EMF) is illustrated in Fig. 6. The back EMF waveform of the AVIPM machine exhibits a notable axis shift compared to the VIPM machine, as shown in Fig. 6 (a), which validates the MFS effect due to the asymmetric flux barriers. In the meantime, the AVIPM machine has a slightly larger main harmonic and a notably lower total harmonic distortion (THD), as shown in Fig. 6 (b). Compared with the VIPM machine, the THD of the AVIPM machine is reduced from 14.1% to 9.3%.

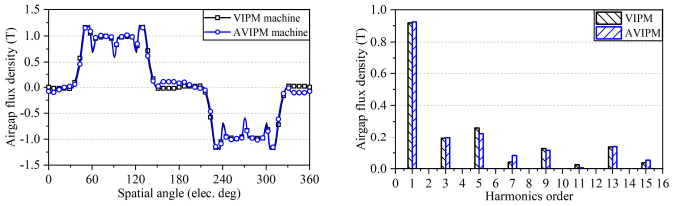

(a) (b)

Fig. 5. Open-circuit airgap flux density of VIPM and AVIPM at 3980 rpm. (a) Waveforms. (b) Harmonics distribution.

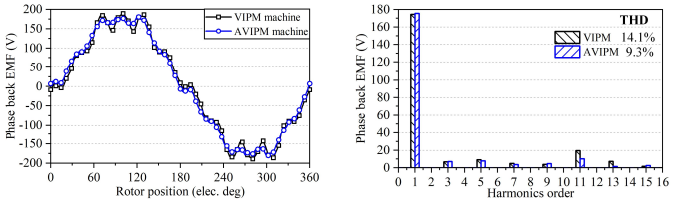

(a) (b)

Fig. 6. Back EMF of Phase A of VIPM and AVIPM at 3980 rpm.(a) Waveforms. (b) Harmonics distribution.

B. The On-load Torque Performance of Machines

The performances of the VIPM machine and the proposed AVIPM machine are listed in Table III, including peak output torque, average torque, torque ripple, and efficiency.

TABLE III
PERFORMANCE OF VIPM MACHINE AND THE PROPOSED AVIPM MACHINE

Machine type	Peak output torque (Nm)	Average torque (Nm)	Torque ripple (%)	Efficiency (%)
VIPM machine	68.74	67.36	6.23	97.17
AVIPM machine	74.74	69.71	15.53	97.29

Fig. 7 shows the on-load torque performance of both machines. As shown in Fig. 7 (a), the maximum torque of the AVIPM machine is 74.74 Nm, which is 8.7% higher than the 68.74 Nm of the VIPM machine. Meanwhile, the current advancing angle at the peak torque of the AVIPM machine is smaller than the VIPM machine due to the MFS effect. The frozen permeability (FP) method is applied to separate the PM torque and reluctance torque accurately [9-10], as shown in Fig. 7 (b). The AVIPM machine has a larger PM torque due to the enhancement of no-load phase back EMF. Meanwhile, the reluctance torque of the AVIPM machine has a significant shifiting compared with that of the VIPM machine. The angle difference between PM torque and reluctance torque is notably reduced, which further improves the peak torque.

The average torque of both machines is shown in Fig. 8 (a). The optimized model of the AVIPM machine has a larger average torque than the VIPM machine. However, the torque enhancement of the AVIPM machine is not significant due to the increase of torque ripple. The average torque is improved by 3.5%. Whereas, the torque ripple is increased from 6.23% to 15.53%, which is a disadvantage of adding asymmetric flux barriers on the rotor core of IPM machines. In addition, the overload capability of the VIPM machine and the AVIPM

machine is compared, which is shown in Fig. 8 (b). When the current density increases from 2 A/mm^2 to 14 A/mm^2, the enhancement of average torque also increases. The ratio of torque increase is elevated from 2.8% at 2 A/mm^2 to 8.3% at 14 A/mm^2. This can be explained by the larger portion of reluctance torque in total torque due to the MFS effect. As shown in (2), the reluctance torque is proportional to the square of the amplitude of phase current, which has a larger increase than the PM torque when the phase current increases. The results show that compared with the conventional VIPM machine, the AVIPM machine has better overload capability.

Moreover, the efficiencies of both machines are evaluated, as shown in Table III. The efficiency is expressed as:

$$\eta = \frac{P_{out}}{P_{in}} \times 100\% = \frac{T_e \omega}{T_e \omega + P_{copper} + P_{core}} \times 100\% \qquad (3)$$

where P_{in}, P_{out}, P_{copper}, and P_{core} are the input power, output power, copper loss, and core loss, respectively. ω is the angular speed of the rotor.

Due to the same stator parameters, the VIPM machine and the AVIPM machine have the same copper loss of 590 W. The core loss is evaluated by using the FEA method. At the rated rotation speed of 3980 rpm, the core loss of the VIPM machine is 226.62 W, and the AVIPM machine has a slightly lower value of 218.45 W. As a result, the efficiency of the AVIPM machine achieves 97.29%, which is slightly higher than the 97.17% of VIPM machine.

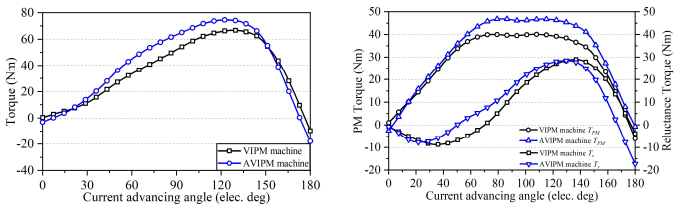

Fig. 7. On-load torque performance of VIPM and AVIPM at 3980 rpm. (a) Torque at different current advancing angles. (b) Separation of PM torque and reluctance torque.

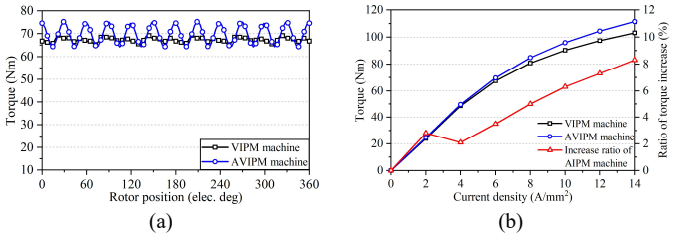

Fig. 8. (a) Average torque. (b) Torque at different current amplitude.

IV. Conclusion

In this study, a novel general pattern of assisted flux barriers is proposed for the optimal design of an AVIPM machine. The proposed general pattern can generate four different types of flux barriers located at different positions on the rotor, which includes most of the existed flux barriers in the literature. A notable advantage is the effect of adding multiple flux barriers on the rotor core can be investigated compared with other studies only studying the impact of a single flux barrier. With the assistance of the optimization method, the position and parameters of flux barriers can be automatically determined. As a result, the optimal design of an AVIPM machine with enhanced torque density can be generated in a short computing time. The optimized AVIPM machine structure reveals that the FB_2 and FB_3 produce the main effect on the torque improvement, and FB_1 and FB_4 have little contribution. The phase back EMF of the AVIPM machine has a slightly higher fundamental harmonic than the VIPM machine and notably lower THD due to the existence of flux barriers. The main function of the MFS effect is improving the peak output torque. The proposed AVIPM machine has a torque enhancement of 8.7%, which is resulted from the increase of PM torque and the shifting of reluctance torque due to the MFS effect. Meanwhile, the proposed AVIPM machine exhibits an improved overload ability. The average torque has a larger enhancement at high current densities due to the increased contribution of the reluctance torque component. Moreover, the efficiency of the proposed machine has a high value of over 97%. However, one disadvantage of the proposed machine is the increased torque ripple due to the flux barriers, which reduces the improvement of average torque.

Acknowledgment

This work was supported by the Research Grant Council of the Hong Kong SAR Government under projects PolyU PolyU152180/19E and PolyU152185/18E.

References

[1] Z. Q. Zhu and D. Howe, "Electrical machines and drives for electric, hybrid, and fuel cell vehicles," *Proc. IEEE*, vol. 95, no. 4, pp. 746–765, Apr. 2007.

[2] Ya Li, Hui Yang, Heyun Lin, Shuhua Fang, and Weijia Wang, "A novel magnet-axis-shifted hybrid permanent magnet machine for electric vehicle applications," *Energies*., vol. 12, no. 4, Art. No. 641, Feb. 2019.

[3] W. Zhao, F. Zhao, T. A. Lipo, and B.-I. Kwon, "Optimal design of a novel V-Type interior permanent magnet motor with assisted barriers for the improvement of torque characteristics," *IEEE Trans. Magn*., vol. 50, no. 11, pp. 1–4, Nov. 2014.

[4] S. Hayslett and E. Strangas, "Design and analysis of aligned axis interior permanent magnet machines considering saturation," in *2019 IEEE Int. Elect. Mach. & Drives Conf. (IEMDC)*, San Diego, CA, USA, May 2019, pp. 686–692.

[5] K. Yamazaki and R. Kondo, "Reduction of cross magnetization in interior permanent magnet synchronous motors with V-Shape magnet configurations by optimizing rotor slits," *in Energy Convers.Congr. and Expo. (ECCE)*, Baltimore, MD, USA, Sep. 2019, pp. 4873–4879.

[6] Y. Xiao, Z. Q. Zhu, J. T. Chen, D. Wu, and L. M. Gong, "A novel V-Shape interior permanent magnet synchronous machine with asymmetric Spoke-type flux barrier," in *2020 Int. Conf. on Elect. Mach. (ICEM)*, Gothenburg, Sweden, Aug. 2020, pp. 382–388.

[7] H. Yang et al., "A Novel Asymmetric-Magnetic-Pole Interior PM Machine With Magnet-Axis-Shifting Effect," *IEEE Trans. on Ind. Applicat*., vol. 57, no. 6, pp. 5927–5938, Nov. 2021.

[8] X. Zhao and S. Niu, "Design and optimization of a new Magnetic-Geared pole-changing hybrid excitation machine," *IEEE Trans. Ind. Electron*., vol. 64, no. 12, pp. 9943–9952, Dec. 2017.

[9] W. Q. Chu and Z. Q. Zhu, "Average torque separation in permanent magnet synchronous machines using frozen permeability," *IEEE Trans. Magn.*, vol. 49, no. 3, pp. 1202–1210, Mar. 2013.

[10] Yongsheng Ge, Hui Yang, Weijia Wang, Heyun Lin, and Ya Li, "A novel interior permanent magnet machine with magnet axis shifted effect for electric vehicle applications," *World Electr. Veh. J*., vol. 12, no. 4, pp. 189, 2021.